Journal of Zhejiang University-SCIENCE A (Applied Physics & Engineering)
ISSN 1673-565X (Print); ISSN 1862-1775 (Online)
www.jzus.zju.edu.cn; www.springerlink.com
E-mail: jzus@zju.edu.cn

Curve smoothing using a continuous function*

Yu-fei WU†1, Liang HE2,3, Zhi-dong LI1

[1]School of Engineering, RMIT University, Carlton, Victoria 3053, Australia
[2]Guangzhou Metro Design and Research Institute Co. Ltd., Guangzhou 510010, China
[3]Department of Architecture and Civil Engineering, City University of Hong Kong, Kowloon, Hong Kong, China
†E-mail: yufei.wu@rmit.edu.au

Received Sept. 16, 2017; Revision accepted Jan. 25, 2018; Crosschecked Mar. 20, 2018

Abstract: Current curve smoothing technologies provide a smoothed curve by joining together separate curves that have certain degrees of continuity at junctions. These technologies have found many applications in science and engineering. However, none of them can provide a smoothed curve using a single continuous function for arbitrary segmental curves. This paper reports a new approach that can be used to construct a single continuous function that joins an arbitrary number of different segmental curves, with the required degree of continuity at all junctions. The smoothness of transition at different junctions can be controlled by separate parameters to suit different needs. The combined continuous function can approach the original segmental functions asymptotically or match the original segmental functions "exactly" inside each segment by adjusting the smoothness parameter. This new approach may also find application outside the scope of curve smoothing/curving fitting in the future.

Key words: Curve smoothing; Curve fitting; Transition curve; Path planning; Tool path
https://doi.org/10.1631/jzus.A1700502 **CLC number:** TV5

1 Introduction

Curve smoothing algorithms convert segmental curves (paths) with discontinuities (such as slope and curvature) at junctions to smooth ones. They are widely used in many fields of science and engineering, such as robot motion planning, machining, computer graphics, pharmacy, and transportation (Cai and Wang, 2009; Huh and Chang, 2014; Roy et al., 2015). The design of smooth transition curves is an important issue in highway path planning and mobile robot design because an "unsmooth" path can cause slippage and over-actuation. Many algorithms have been developed for path smoothing to suit different needs (Fraichard and Scheuer, 2004; Magid et al., 2006; Yang and Sukkarieh, 2010; Huh and Chang, 2014). In machining, the most common linear tool path introduces tangent and curvature discontinuities at segment junctions, causing feed fluctuation, decrease of surface quality, and machine efficiency, particularly when high-speed and high-accuracy are required. Various path smoothing algorithms have been developed to resolve the problem, including off-line post-processing, online number control (NC) interpolation, interpolation with a parametric curve such as Bezier, non-uniform rational basis spline (NURBS), Hermite, and B-spline curves that have the characteristic of C^2 continuity (Erkorkmaz and Altintas, 2001; Yeh and Hsu, 2002; Nam and Yang, 2004; Liu et al., 2005; Yang and Chen, 2006; Lin et al., 2007; Yau and Wang, 2007; Walton and Meek, 2009, 2010; Wang and Yau, 2009; Emami and Arezoo, 2010; Feng et al., 2010; Pateloup et al., 2010; Zhang et al., 2011).

Smoothed paths are currently generated as a set of discrete data points or separate functions with

* Project supported by the National Natural Science Foundation of China (No. 51378449)
ORCID: Yu-fei WU, https://orcid.org/0000-0002-3970-3999

certain degrees of continuity at junctions. The smoothing algorithms can provide good control of curvature profile of a smoothed curve, but ignore the deviation of the smoothed paths from the original paths. Ideal paths should have the following characteristics simultaneously (Pateloup et al., 2010): (1) limitation of approximation error, (2) continuity of tangency and curvature, (3) suppression of path oscillations, and (4) control of curvature profile. Current smoothing algorithms find these requirements difficult to satisfy simultaneously. Furthermore, all smoothed paths/curves are segmental or piecewise that cannot be described by one continuous function.

In this work, a special curve smoothing approach is developed that (1) provides smooth transition at all junctions with controllable transition sharpness or curvature, (2) asymptotically approaches all original segments that are given by any continuous function, and (3) is given by one single continuous function in the whole domain. As far as we know, it is the first time that such an approach/function is reported in the literature. The application of this approach/function may not be limited to curve/path smoothing.

2 A general two-function multiplication method

2.1 Regional variables

Define two regional variables as

$$t_r = \frac{x}{\left(1+\left(\frac{x}{x_0}\right)^n\right)^{1/n}}, \tag{1}$$

$$t_l = (x+\delta)\left(1+\left(\frac{x_0}{x+\delta}\right)^n\right)^{1/n}, \tag{2}$$

where x is the global variable in the domain $(0, b)$ and x_0 is a particular value of x inside $(0, b)$ that divides the whole domain into two regions; n is a constant that affects the smoothness of transition (Fig. 1); δ is a small constant that is used to avoid singularity of t_l at x=0.

The two regional variables are shown in Fig. 1. It can be seen that t_r takes the value of x in its effective region $(0, x_0)$, and becomes a constant x_0 outside it, while t_l is the opposite, being a constant x_0 in $(0, x_0)$ and x in (x_0, b). The bigger the parameter n is, the sharper the transition becomes between the two regions. In general, a value greater than 10 should be used for n to make a clear transition. It is noted that a function similar to Eq. (1) was used by others in modeling stress-strain curves (Giuffre and Pinto, 1970; Richard and Abbott, 1975).

If the variable x is defined in a more general domain (a, b), a variable substitution of ξ=$x-a$ can be used to change the x domain to a ξ domain of $(0, b-a)$.

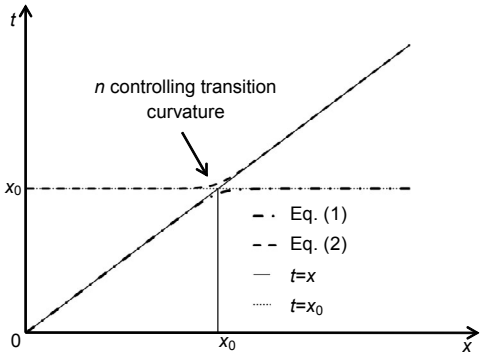

Fig. 1 Regional variables for two-segment function

2.2 Regional functions and combined function

For a general function given by

$$y = f(x) = y_0 \cdot \bar{f}(x), \tag{3}$$

where $\bar{f}(x)$ is a normalized function with its value equal to 1 at x_0, and y_0 is the value of y at x_0. Replacing x with t_r and t_l respectively gives

$$y_1 = y_0 \cdot \bar{f}(t_r), \tag{4}$$

$$y_2 = y_0 \cdot \bar{f}(t_l). \tag{5}$$

Eq. (4) is equal to Eq. (3) approximately (the difference depends on the value of n) in $(0, x_0)$ and becomes a constant outside the region. Eq. (5) is the opposite and can be used to represent $f(x)$ in the region (x_0, b). A very useful feature of Eqs. (4) and (5) is that they are only regional functions inside their own effective regions and do not affect others outside the regions.

For a typical two-part function that has distinctive shapes in the two sides as shown in Fig. 2, assume

the function on the left hand side is given by $y_1 = y_0 \cdot \bar{f}_1(x)$ and that on the right hand side is given by $y_2 = y_0 \cdot \bar{f}_2(x)$. Let

$$y_1 = y_0 \cdot \bar{f}_1(t_r)\bar{f}_2(t_1). \tag{6}$$

The combined function y is y_1 in $(0, x_0)$ and y_2 in (x_0, b). In the transition zone around x_0 the function is smooth and mathematically continuous.

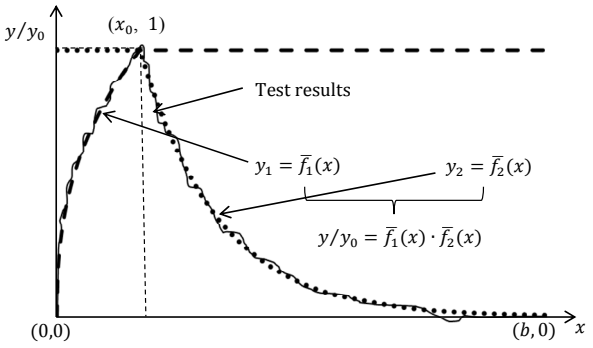

Fig. 2 Two-function multiplication method

2.3 Examples of two-segment functions

Hognestad (1951) proposed a stress-strain relationship for concrete, which was adopted by many researchers to describe the stress-strain relationship of fibre-reinforced polymer (FRP)-confined concrete.

$$f_c = \begin{cases} f_{co}\left[\dfrac{2\varepsilon_c}{\varepsilon_{co}} - \left(\dfrac{\varepsilon_c}{\varepsilon_{co}}\right)^2\right], & \varepsilon_c \le \varepsilon_{co}, \\ f_{co} + E_2(\varepsilon_c - \varepsilon_{co}), & \varepsilon_c > \varepsilon_{co}, \end{cases} \tag{7}$$

where f_c and ε_c are the stress and strain of concrete, respectively, and $(f_{co}, \varepsilon_{co})$ is the coordinate of the transition point shown in Fig. 3; E_2 is the slope of the second part that is represented by a straight line. By applying Eq. (6), we have

$$f_c = \left[\frac{2t_r}{\varepsilon_{co}} - \left(\frac{t_r}{\varepsilon_{co}}\right)^2\right] \cdot \left[f_{co} + E_2(t_1 - \varepsilon_{co})\right], \tag{8a}$$

$$t_r = \frac{\varepsilon_c}{\left(1 + \left(\dfrac{\varepsilon_c}{\varepsilon_{co}}\right)^n\right)^{1/n}}, \tag{8b}$$

$$t_1 = (\varepsilon_c + \delta)\left(1 + \left(\frac{\varepsilon_{co}}{\varepsilon_c + \delta}\right)^n\right)^{1/n}. \tag{8c}$$

Using n=10 and δ=0.001, Eq. (8a) is shown in Fig. 3. It is clear that Eq. (8a) is essentially identical to Eq. (7), but it is a mathematically continuous function.

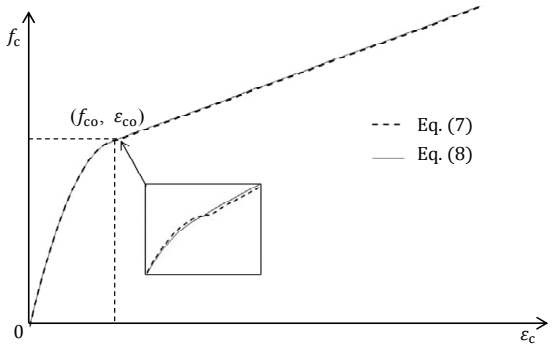

Fig. 3 Hognestad stress-strain model

The second example is an interfacial bond-slip relationship (Pan and Wu, 2014) for externally bonded reinforcement-to-concrete interface, as given by

$$\tau = \begin{cases} \tau_{max}\left(\dfrac{s}{s_0}\right)^{\alpha}, & s \le s_0, \\ \tau_{max}\exp[-\beta(s - s_0)], & s > s_0, \end{cases} \tag{9}$$

where τ and s are the interfacial bond stress and slip, respectively, with the peak point at (s_0, τ_{max}); τ_{max} is the maximum bond stress; α and β are two parameters controlling the shape of the curves. Using the two-function multiplication method, Eq. (9) is converted to a continuous function:

$$\tau = \tau_{max}\left(\frac{t_r}{s_0}\right)^{\alpha}\exp[-\beta(t_1 - s_0)], \tag{10a}$$

$$t_r = \frac{s}{\left(1 + \left(\dfrac{s}{s_0}\right)^n\right)^{1/n}}, \tag{10b}$$

$$t_1 = (s + \delta)\left(1 + \left(\frac{s_0}{s + \delta}\right)^n\right)^{1/n}, \tag{10c}$$

when n=35 and δ=0.0001, Eq. (9) and Eq. (10a) are shown and compared in Fig. 4.

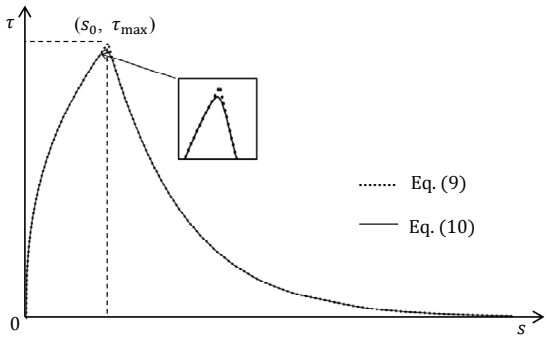

Fig. 4 Discontinuous bond-slip relationship

3 Multiple-segment functions

When a two-segment function is combined with another single-segment function using the two-function multiplication method, it produces a three-segment function. This process can continue to produce an m-segment function. Generally, an (m+n)-segment function can be produced by combining an m-segment function f_m with an n-segment function f_n, or

$$f(x)=y_0\cdot\overline{f}_m(t_r)\overline{f}_n(t_1). \tag{11}$$

However, the process to produce a function with multiple segments using Eq. (11) is tedious. A simpler way to produce a multiple-segment function is by introducing a more general regional variable that is equal to x in a sub-domain (x_i, x_{i+1}) and becomes constant outside the region. Such a regional variable is given by

$$\begin{aligned}t_i&=\frac{t_r(x_{i+1})t_1(x_i)}{x}\\&=\frac{x+\delta}{\left(1+\left(\dfrac{x}{x_{i+1}}\right)^n\right)^{1/n}}\left(1+\left(\frac{x_i}{x+\delta}\right)^n\right)^{1/n},\end{aligned} \tag{12}$$

where x is the global variable in the domain (0, b), and x_i and x_{i+1} are two boundary values of the sub-domain. Eq. (12) is depicted in Fig. 5. It can be seen that t_i takes the value of x in its sub-domain (x_i, x_{i+1}), and a constant value of x_i in (0, x_i) and another value of x_{i+1} in (x_{i+1}, b). When x_i is equal to 0, Eq. (12) degenerates to Eq. (1). Similarly, Eq. (12) reduces to Eq. (2) when x_{i+1} is equal to b.

With the regional variable given by Eq. (12), any function $f(t_i)$ presents in its original form $f(x)$ inside its sub-domain and becomes constant outside it. For a discontinuous multiple-segment function with its ith segment,

$$y_i=y_{0,i}\cdot\overline{f}_l(x), \tag{13}$$

where $y_{0,i}$ is the y value of the function at x=x_i, and $\overline{f}_l(x)$ is a normalized function with its value equal to 1 at x_i, the general m-segment continuous function can simply be given by

$$f(x)=y_{0,1}\cdot\overline{f}_1(t_1)\overline{f}_2(t_2)\cdots\overline{f}_l(t_i)\cdots\overline{f}_m(t_m). \tag{14}$$

Note that different values of n or n_i can be used in Eq. (12) so that the sharpness of turning at different junctions can be chosen separately based on needs.

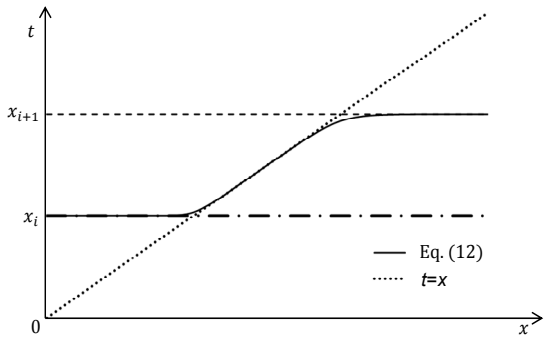

Fig. 5 General regional variable for sub-domain

Examples of multiple-segment functions are given as follows.

1. Stress-strain relationship of steel bar

The typical stress-strain relationship of a hot-rolled steel bar (Park and Paulay, 1975) is shown in Fig. 6. This constitutive relationship has four parts and regional variables can be applied to produce a continuous function. The elastic and perfectly plastic parts are given by

$$\sigma=\begin{cases}E\varepsilon, & 0\le\varepsilon<\varepsilon_1,\\ \sigma_y, & \varepsilon_1\le\varepsilon\le\varepsilon_2,\end{cases} \tag{15}$$

where σ and ε are the stress and strain, respectively; E

is the Young's modulus and σ_y is the yield strength; ε_1 and ε_2 give the starting and end points of the yield plateau, respectively.

Eq. (15) can easily be transformed into a two-segment function using the two-function multiplication method:

$$\sigma(\varepsilon)=\frac{E\varepsilon}{\left(1+\left(\frac{\varepsilon}{\varepsilon_1}\right)^n\right)^{1/n}}. \tag{16}$$

The third and fourth parts of the curve can be provided by

$$\sigma(\varepsilon)=\sigma_u-A(\varepsilon_u-\varepsilon)^P, \tag{17}$$

$$\sigma(\varepsilon)=\sigma_u-B(\varepsilon-\varepsilon_u)^Q, \tag{18}$$

where A and B are constants given by

$$A=\frac{\sigma_u-\sigma_y}{(\varepsilon_u-\varepsilon_2)^P}, \tag{19a}$$

$$B=\frac{\sigma_u-\sigma_m}{(\varepsilon_m-\varepsilon_u)^Q}, \tag{19b}$$

where σ_u and ε_u are the stress and strain of the peak point, respectively; σ_m and ε_m are the stress and strain of the end point, respectively.

Applying Eq. (14) to the above functions gives

$$\sigma(\varepsilon)=\frac{E\varepsilon}{\left(1+\left(\frac{\varepsilon}{\varepsilon_1}\right)^n\right)^{1/n}} \times\frac{\sigma_u-A(\varepsilon_u-t_3)^P}{\sigma_y}\cdot\frac{\sigma_u-B(t_4-\varepsilon_u)^Q}{\sigma_u}, \tag{20a}$$

$$t_3=\frac{\varepsilon+\delta}{\left(1+\left(\frac{\varepsilon}{\varepsilon_u}\right)^n\right)^{1/n}}\left(1+\left(\frac{\varepsilon_2}{\varepsilon+\delta}\right)^n\right)^{1/n}, \tag{20b}$$

$$t_4=\frac{\varepsilon+\delta}{\left(1+\left(\frac{\varepsilon}{\varepsilon_m}\right)^n\right)^{1/n}}\left(1+\left(\frac{\varepsilon_u}{\varepsilon+\delta}\right)^n\right)^{1/n}. \tag{20c}$$

The continuous function Eq. (20a) is depicted in Fig. 6, where the parameters of n=20 and δ=0.0001 are used.

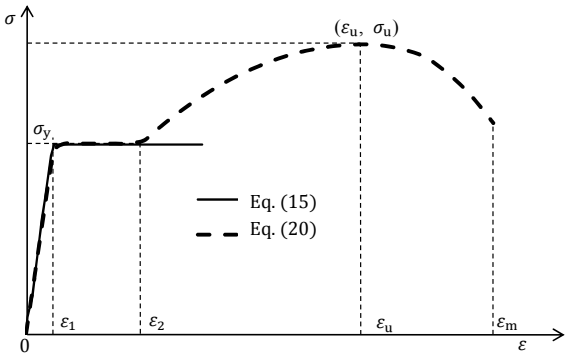

Fig. 6 Stress-strain relationship of steel bar

2. Bond-slip relationship of reinforced concrete

The well-known Bertero, Popov, and Eligehausen (BPE) model (CEB, 1993) that is used as the bond-slip relationship for a reinforcement bar-concrete interface is given by Eq. (21) and shown in Fig. 7a.

$$\tau=\begin{cases}\tau_{max}\left(\dfrac{s}{s_1}\right)^{0.4}, & 0\le s\le s_1,\\ \tau_{max}, & s_1<s\le s_2,\\ \tau_{max}-(\tau_{max}-\tau_f)\left(\dfrac{s-s_2}{s_3-s_2}\right), & s_2<s\le s_3,\\ \tau_f, & s_3<s,\end{cases} \tag{21}$$

where s_1, s_2, and s_3 are the values of slip at the first, second, and third turning points of the curve, respectively; τ_f is the residual stress.

Using the multiple-segment function, the continuous BPE model is given by

$$\tau=\left(\frac{t_1}{s_1}\right)^{0.4}\left[\tau_{max}-(\tau_{max}-\tau_f)\left(\frac{t_3-s_2}{s_3-s_2}\right)\right], \tag{22a}$$

$$t_1=\frac{s}{\left(1+\left(\frac{s}{s_1}\right)^n\right)^{1/n}}, \tag{22b}$$

$$t_3=\frac{s+\delta}{\left(1+\left(\frac{s}{s_3}\right)^n\right)^{1/n}}\left(1+\left(\frac{s_2}{s+\delta}\right)^n\right)^{1/n}. \tag{22c}$$

There are only two segments in Eq. (22a) because the second and fourth parts are constants and equal to 1 after normalization.

In fact, a simpler continuous function can be derived for the BPE model by another method. For the first ascending part and the second peak plateau at τ_{max}, one can use one hyperbolic tangent function to simulate the curve, i.e.

$$\tau(s)=\tau_{\max}\tanh(E_1 s), \tag{23}$$

where E_1 is the initial slope at s=0. The descending branch (the third part) and the residual flat plateau (the fourth part) can also be given as another hyperbolic tangent function:

$$\tau(s)=\frac{\tau_{\max}-\tau_{\mathrm{f}}}{2}\tanh\left[-E_2\left(s-\frac{s_2+s_3}{2}\right)\right]+\frac{\tau_{\max}+\tau_{\mathrm{f}}}{2}, \tag{24}$$

where E_2 is the slope of the descending branch at s=(s_2+s_3)/2. The curves of Eq. (23) and Eq. (24) are shown in Fig. 7b by the dotted line and dashed line, respectively.

Using the two-function multiplication method, one gets

$$\tau(s)=\tanh(E_1 s)\times\left\{\frac{\tau_{\max}-\tau_{\mathrm{f}}}{2}\tanh\left[-E_2\left(s-\frac{s_2+s_3}{2}\right)\right]+\frac{\tau_{\max}+\tau_{\mathrm{f}}}{2}\right\}. \tag{25}$$

Eq. (25) is shown in Fig. 7a in comparison with the original BPE model Eq. (21) and Eq. (22), where n=50, δ=0.0001, E_1=1, and E_2=0.5. As both Eq. (23) and Eq. (24) are constant outside their own effective region (Fig. 7b), the regional variables are not required in Eq. (25).

3. Constitutive relationship of steel-FRP composite bar (SFCB)

A special composite bar, namely SFCB bar (Wu et al., 2012), which is made from steel and FRP composites, is shown in Fig. 8. As steel yields and FRP materials break at different strain values, the stress-strain relationship of the composite bar has five turning points and six segments, which are given by the following equation:

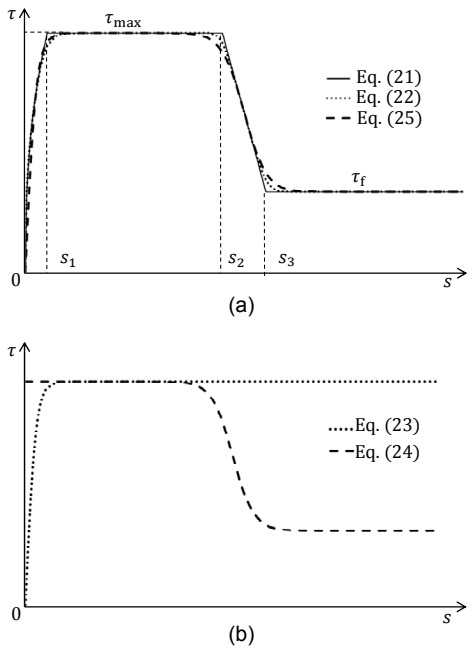

Fig. 7 Bond-slip relationship for concrete-rebar interface
(a) Discontinuous and continuous models; (b) Hyperbolic tangent functions

$$\sigma=\begin{cases}E_1\varepsilon, & 0\le\varepsilon<\varepsilon_1,\\ f_1+E_2(\varepsilon-\varepsilon_1), & \varepsilon_1\le\varepsilon<\varepsilon_2,\\ f_{2\mathrm{d}}+E_3(\varepsilon-\varepsilon_2), & \varepsilon_2\le\varepsilon<\varepsilon_3,\\ f_{3\mathrm{d}}, & \varepsilon_3\le\varepsilon,\end{cases} \tag{26}$$

where E_1, E_2, and E_3 are the slopes of the first, second, and third inclined lines, respectively; ε_1, ε_2, and ε_3 are the strains of the end points of the first, second, and third inclined lines, respectively; f_1, $f_{2\mathrm{d}}$, and $f_{3\mathrm{d}}$ are the stresses of the starting points of the second and third inclined lines, and residual plateau, respectively.

Dividing the curve in Fig. 8a into six parts, the function of first, second, and third ascending parts can be described by its original functions in Eq. (26). However, the two vertical drops have no expression. To make the function continuous, the following two expressions are used for these two parts:

$$\sigma=\frac{f_{2\mathrm{d}}-f_{2\mathrm{u}}}{\Delta}(\varepsilon-\varepsilon_2-\Delta)+f_{2\mathrm{d}}, \tag{27}$$

$$\sigma=\frac{f_{3\mathrm{d}}-f_{3\mathrm{u}}}{\Delta}(\varepsilon-\varepsilon_3-\Delta)+f_{3\mathrm{d}}, \tag{28}$$

where Δ is a small constant to allow for the x coordinate at the lower point of the vertical drop to be slightly

larger than that at the upper point, and can approach zero; f_{2u} and f_{3u} are the stresses of the end points of the second and third inclined lines, respectively.

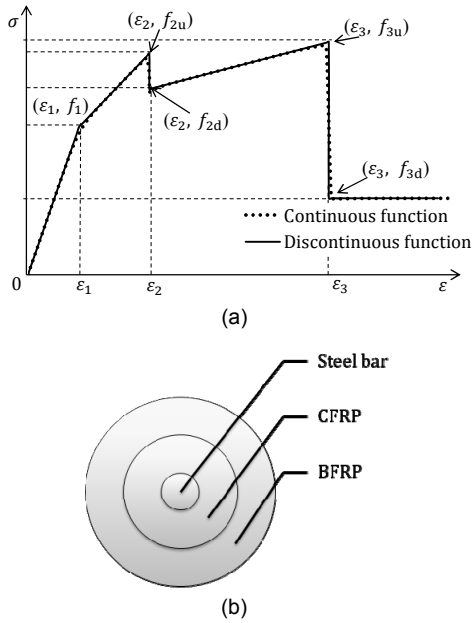

Fig. 8 Constitutive relationship of SFCB
(a) Stress-strain models; (b) Cross-section. CFRP: carbon fibre-reinforced polymer; BFRP: basalt fibre-reinforced polymer

Using Eq. (14), the continuous stress-strain model is given by

$$\begin{aligned}\sigma = {} & E_1 t_1 \frac{f_1 + E_2(t_2-\varepsilon_1)}{f_1} \\ & \times \frac{\frac{f_{2d}-f_{2u}}{\Delta}(t_3-\varepsilon_2-\Delta)+f_{2d}}{f_{2u}} \\ & \times \frac{f_{2d}+E_3(t_4-\varepsilon_2)}{f_{2d}} \\ & \times \frac{\frac{f_{3d}-f_{3u}}{\Delta}(t_5-\varepsilon_3-\Delta)+f_{3d}}{f_{3u}},\end{aligned} \tag{29a}$$

$$t_1 = \frac{\varepsilon}{\left(1+\left(\frac{\varepsilon}{\varepsilon_1}\right)^n\right)^{1/n}}, \tag{29b}$$

$$t_2 = \frac{\varepsilon+\delta}{\left(1+\left(\frac{\varepsilon}{\varepsilon_2}\right)^n\right)^{1/n}}\left(1+\left(\frac{\varepsilon_1}{\varepsilon+\delta}\right)^n\right)^{1/n}, \tag{29c}$$

$$t_3 = \frac{\varepsilon+\delta}{\left(1+\left(\frac{\varepsilon}{\varepsilon_2+\Delta}\right)^n\right)^{1/n}}\left(1+\left(\frac{\varepsilon_2}{\varepsilon+\delta}\right)^n\right)^{1/n}, \tag{29d}$$

$$t_4 = \frac{\varepsilon+\delta}{\left(1+\left(\frac{\varepsilon}{\varepsilon_3}\right)^n\right)^{1/n}}\left(1+\left(\frac{\varepsilon_2+\Delta}{\varepsilon+\delta}\right)^n\right)^{1/n}, \tag{29e}$$

$$t_5 = \frac{\varepsilon+\delta}{\left(1+\left(\frac{\varepsilon}{\varepsilon_3+\Delta}\right)^n\right)^{1/n}}\left(1+\left(\frac{\varepsilon_3}{\varepsilon+\delta}\right)^n\right)^{1/n}. \tag{29f}$$

Eqs. (26) and (29a) are shown in Fig. 8a by the solid line and dotted line, respectively, where n=15, δ=0.001, and Δ=0.01.

4 Curvature of combined function

The variation of curvature is an important consideration in curve smoothing. The curvature at a junction is not only related to original curves at the two sides of the junction but also related to the sharpness of transition that is controlled by n in Eq. (12). The curvature at a typical junction is studied in this section through the case of the two-function multiplication method.

Based on Eqs. (1) and (2), we obtain the first and second derivatives of t_r and t_l with respect to x as follows:

$$t_r' = \frac{1}{\left(1+\left(\frac{x}{x_0}\right)^n\right)^{1+1/n}}, \tag{30a}$$

$$t_l' = \left(1+\left(\frac{x_0}{x+\delta}\right)^n\right)^{1/n-1}, \tag{30b}$$

$$t_r'' = \frac{-n-1}{\left(1+\left(\frac{x}{x_0}\right)^n\right)^{2+1/n}}\frac{x^{n-1}}{x_0^n}, \tag{30c}$$

$$t_l'' = (n-1)\left(1+\left(\frac{x_0}{x+\delta}\right)^n\right)^{1/n-2}\frac{x_0^n}{(x+\delta)^{n+1}}. \tag{30d}$$

The curvature of the combined function, Eq. (6), is given by

$$k=\frac{y''}{\left(1+(y')^2\right)^{3/2}}, \tag{31}$$

where the first derivative and the second derivative of y with respect to x are given by

$$y'=y_0\left[\bar{f}_1'(t_\mathrm{r})\cdot t_\mathrm{r}'\cdot\bar{f}_2(t_1)+\bar{f}_1(t_\mathrm{r})\cdot t_1'\cdot\bar{f}_2'(t_1)\right], \tag{32}$$

$$\begin{aligned}y''=y_0\Big[&\bar{f}_1''(t_\mathrm{r})\cdot(t_\mathrm{r}')^2\cdot\bar{f}_2(t_1)\\&+\bar{f}_1'(t_\mathrm{r})\cdot t_\mathrm{r}''\cdot\bar{f}_2(t_1)+2\bar{f}_1'(t_\mathrm{r})\cdot t_\mathrm{r}'\cdot t_1'\cdot\bar{f}_2'(t_1)\\&+\bar{f}_1(t_\mathrm{r})\cdot t_1''\cdot\bar{f}_2(t_1)+\bar{f}_1(t_\mathrm{r})\cdot(t_1')^2\cdot\bar{f}_2''(t_1)\Big].\end{aligned} \tag{33}$$

The expressions of $\bar{f}_1'(t_\mathrm{r})$, $\bar{f}_1''(t_\mathrm{r})$, $\bar{f}_2'(t_1)$, and $\bar{f}_2''(t_1)$ are only related to the original part functions $f_1(x)$ and $f_2(x)$. It is obvious that the curvature of the combined function or Eq. (31) is continuous in the whole domain as long as the original functions are C^2 differentiable. Based on Eqs. (31)–(33), one can see that the curvature of the transition part is not only related to the regional variables Eqs. (1) and (2), but also related to the original part functions.

A typical linear tool path problem is studied herein, as shown in Fig. 9. Two linear part functions meet at the point (1, 1) with an angle of θ between them. The slopes of these two curves are $-k_1$ and k_1, respectively, where $k_1=\cot(\theta/2)$. The part functions of these two lines are given by (Fig. 9)

$$\bar{f}_1(t_\mathrm{r})=1-k_1(t_\mathrm{r}-1), \tag{34}$$

$$\bar{f}_2(t_1)=1+k_1(t_1-1). \tag{35}$$

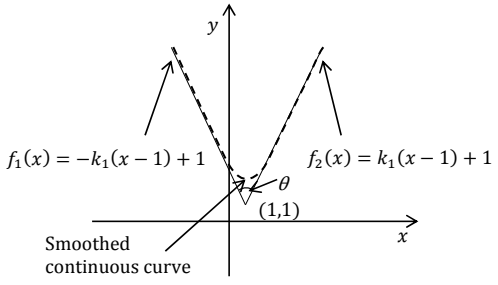

Fig. 9 Smoothing of two linear functions

As the values of $\bar{f}_1'(t_\mathrm{r})$, $\bar{f}_1''(t_\mathrm{r})$, $\bar{f}_2'(t_1)$, and $\bar{f}_2''(t_1)$ in Fig. 9 are equal to $-k_1$, k_1, 0, and 0, respectively, Eqs. (32) and (33) are simplified to:

$$y'=y_0\left[-k_1t_\mathrm{r}'\bar{f}_2(t_1)+k_1t_1'\bar{f}_1(t_\mathrm{r})\right], \tag{36}$$

$$y''=y_0\left[-k_1t_\mathrm{r}''\bar{f}_2(t_1)-2k_1^2t_\mathrm{r}'t_1'+k_1t_1''\bar{f}_1(t_\mathrm{r})\right]. \tag{37}$$

The maximum curvature of the transition curve occurs at the point of x=1 and the value of the maximum curvature is given by Eq. (31) when x=1:

$$k_\mathrm{m}=\frac{y''\big|_{x=1}}{\left(1+\left(y'\big|_{x=1}\right)^2\right)^{3/2}}. \tag{38}$$

Substituting x=1 and x_0=1 into Eq. (1) and Eq. (2), and letting δ=0, one gets:

$$t_\mathrm{r}\big|_{x=1}=2^{-1/n}, \tag{39}$$

$$t_1\big|_{x=1}=2^{1/n}. \tag{40}$$

Substituting Eq. (39) and Eq. (40) into Eq. (34) and Eq. (35), respectively, gives:

$$\bar{f}_1(t_\mathrm{r})\big|_{x=1}=1-k_1(2^{-1/n}-1), \tag{41}$$

$$\bar{f}_2(t_1)\big|_{x=1}=1+k_1(2^{1/n}-1). \tag{42}$$

Letting x=1 and δ=0 in Eqs. (30a)–(30d), one gets:

$$t_\mathrm{r}'\big|_{x=1}=2^{-1-1/n}, \tag{43a}$$

$$t_1'\big|_{x=1}=2^{1/n-1}, \tag{43b}$$

$$t_\mathrm{r}''\big|_{x=1}=(-n-1)2^{-2-1/n}, \tag{43c}$$

$$t_1''\big|_{x=1}=(n-1)2^{1/n-2}. \tag{43d}$$

Substituting Eqs. (41), (42), and (43a)–(43d) into Eq. (36) and Eq. (37) and considering y_0=1 (Fig. 9) gives:

$$y'=k_1(2^{1/n-1}-2^{-1-1/n})+k_1^2(2^{-1-1/n}+2^{1/n-1}-1), \tag{44}$$

$$y''=k_1(1-k_1)(n+1)2^{-2-1/n}+k_1(1+k_1)(n-1)2^{1/n-2}. \tag{45}$$

Substituting Eqs. (44) and (45) into Eq. (38) gives the maximum curvature:

$$k_{\mathrm{m}}=\frac{k_1(1-k_1)(n+1)2^{-2-1/n}+k_1(1+k_1)(n-1)2^{1/n-2}}{\left\{1+\left[k_1(2^{1/n-1}-2^{-1-1/n})+k_1^2(2^{-1-1/n}+2^{1/n-1}-1)\right]^2\right\}^{3/2}}. \tag{46}$$

It can be seen from Eq. (46) that both k_1 and n affect the peak curvature and at smaller θ the curvature increases faster when n increases, as shown in Fig. 10.

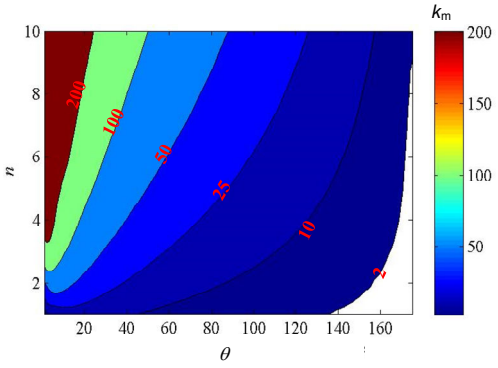

Fig. 10 Relationship between k_{m}, n, and θ

5 Conclusions

A function multiplication method is developed in this work to convert any discontinuous segmental curve into a continuous one. The key of the method is the introduction of a regional variable that equals the original variable in its sub-domain and becomes a constant outside the region. With this regional variable replacing the original, any function takes its original form inside its sub-domain and turns to a constant outside it to become a regional function. Therefore, a multiple-segment discontinuous curve can be converted to a continuous function simply by multiplication of all the regional functions.

It is noted that the smoothed continuous curve using this method does not oscillate at all because of the smooth regional variable used as shown in Fig. 5. By using this regional variable, each segment of curve retains its original shape inside its own sub-domain. In between two sub-domains, a smooth transition is provided with the required degree of smoothness controlled by a smoothness parameter n_i for junction i. Therefore, there is no oscillation problem with this approach.

Continuity of a curve not only brings convenience in scientific studies and engineering applications, but also overcomes difficulties caused by mathematical discontinuity in analytical studies and numerical simulations. The use of this method can extend the applicability of some general and popular tools, such as the Taylor series and the Newton-Raphson method, to problems that were previously inapplicable due to discontinuity or inexistence of derivatives at discontinuous joints. It can bring convenience in engineering computation and computer programming to avoid dividing functions into sub-domains. It can also be used in computer-aided design (CAD) and computer-aided manufacturing (CAM) where curve fitting is required to smooth transition zones. In fact, the method developed in this work provides a general mathematical tool that can be used in all scientific and engineering work.

References

Cai HH, Wang GJ, 2009. A new method in highway route design: joining circular arcs by a single C-Bézier curve with shape parameter. *Journal of Zhejiang University-SCIENCE A*, 10(4):562-569. https://doi.org/10.1631/jzus.A0820267

CEB (Comite Euro-International du Beton), 1993. CEB-FIP Model Code 1990: Design Code FIB-Fédération Internationale du Beton.

Emami MM, Arezoo B, 2010. A look-ahead command generator with control over trajectory and chord error for NURBS curve with unknown arc length. *Computer-Aided Design*, 42(7):625-632. https://doi.org/10.1016/j.cad.2010.04.001

Erkorkmaz K, Altintas Y, 2001. High speed CNC system design. Part I: jerk limited trajectory generation and quintic spline interpolation. *International Journal of Machine Tools and Manufacture*, 41(9):1323-1345. https://doi.org/10.1016/S0890-6955(01)00002-5

Feng J, Li Y, Wang Y, et al., 2010. Design of a real-time adaptive NURBS interpolator with axis acceleration limit. *The International Journal of Advanced Manufacturing Technology*, 48(1-4):227-241. https://doi.org/10.1007/s00170-009-2261-y

Fraichard T, Scheuer A, 2004. From Reeds and Shepp's to continuous-curvature paths. *IEEE Transactions on Robotics*, 20(6):1025-1035. https://doi.org/10.1109/TRO.2004.833789

Giuffre A, Pinto PE, 1970. Il comportamento del cemento armato per sollecitazioni cicliche di forte intensita. *Giornale del Genio Civile*, 5:391-408 (in Italian).

Hognestad E, 1951. A Study of Combined Bending and Axial

Load in Reinforced Concrete Members. Bulletin Series No. 399, Engineering Experiment Station, University of Illinois, Urbana, USA.

Huh UY, Chang SR, 2014. A G^2 continuous path-smoothing algorithm using modified quadratic polynomial interpolation. *International Journal of Advanced Robotic Systems*, 11(2):1-11. https://doi.org/10.5772/57340

Lin MT, Tsai MS, Yau HT, 2007. Development of a dynamics-based NURBS interpolator with real-time look-ahead algorithm. *International Journal of Machine Tools and Manufacture*, 47(15):2246-2262. https://doi.org/10.1016/j.ijmachtools.2007.06.005

Liu X, Ahmad F, Yamazaki K, et al., 2005. Adaptive interpolation scheme for NURBS curves with the integration of machining dynamics. *International Journal of Machine Tools and Manufacture*, 45(4-5):433-444. https://doi.org/10.1016/j.ijmachtools.2004.09.009

Magid E, Keren D, Rivlin E, et al., 2006. Spline-based robot navigation. Proceedings of the 2006 IEEE/RSJ International Conference on Intelligent Robots and Systems, p.2296-2301.

Nam SH, Yang MY, 2004. A study on a generalized parametric interpolator with real-time jerk-limited acceleration. *Computer-Aided Design*, 36(1):27-36. https://doi.org/10.1016/S0010-4485(03)00066-6

Pan J, Wu YF, 2014. Analytical modeling of bond behavior between FRP plate and concrete. *Composites Part B: Engineering*, 61:17-25. https://doi.org/10.1016/j.compositesb.2014.01.026

Park R, Paulay T, 1975. Reinforced Concrete Structures. John Wiley & Sons, New York.

Pateloup V, Duc E, Ray P, 2010. Bspline approximation of circle arc and straight line for pocket machining. *Computer-Aided Design*, 42(9):817-827. https://doi.org/10.1016/j.cad.2010.05.003

Richard RM, Abbott BJ, 1975. Versatile elastic-plastic stress-strain formula. *Journal of the Engineering Mechanics Division*, 101:511-515.

Roy R, Bodduna K, Kumari N, et al., 2015. A fast and efficient mesh smoothing algorithm for 3D graphical models using cubic B-splines. *In*: Information Systems Design and Intelligent Applications. Springer, New Delhi, India, p.467-474. https://doi.org/10.1007/978-81-322-2247-7_48

Walton DJ, Meek DS, 2009. G^2 blends of linear segments with cubics and pythagorean-hodograph quintics. *International Journal of Computer Mathematics*, 86(9):1498-1511. https://doi.org/10.1080/00207160701828157

Walton DJ, Meek DS, 2010. Cubic Bézier spiral segments for planar G^2 curve design. Proceedings of the 7th International Conference on Computer Graphics, Virtual Reality, Visualisation and Interaction in Africa, ACM, p.21-26.

Wang JB, Yau HT, 2009. Real-time NURBS interpolator: application to short linear segments. *International Journal of Advanced Manufacturing Technology*, 41(11-12): 1169-1185. https://doi.org/10.1007/s00170-008-1564-8

Wu G, Sun ZY, Wu ZS, et al., 2012. Mechanical properties of steel-FRP composite bars (SFCBs) and performance of SFCB reinforced concrete structures. *Advances in Structural Engineering*, 15(4):625-636. https://doi.org/10.1260/1369-4332.15.4.625

Yang K, Sukkarieh S, 2010. An analytical continuous-curvature path-smoothing algorithm. *IEEE Transactions on Robotics*, 26(3):561-568. https://doi.org/10.1109/TRO.2010.2042990

Yang X, Chen ZC, 2006. A practicable approach to G^1 biarc approximations for making accurate, smooth and non-gouged profile features in CNC contouring. *Computer-Aided Design*, 38(11):1205-1213. https://doi.org/10.1016/j.cad.2006.07.006

Yau HT, Wang JB, 2007. Fast Bezier interpolator with real-time look ahead function for high-accuracy machining. *International Journal of Machine Tools and Manufacture*, 47(10):1518-1529. https://doi.org/10.1016/j.ijmachtools.2006.11.010

Yeh SS, Hsu PL, 2002. Adaptive-feedrate interpolation for parametric curves with a confined chord error. *Computer-Aided Design*, 34(3):229-237. https://doi.org/10.1016/S0010-4485(01)00082-3

Zhang LB, You YP, He J, et al., 2011. The transition algorithm based on parametric spline curve for high-speed machining of continuous short line segments. *International Journal of Advanced Manufacturing Technology*, 52(1-4):245-254. https://doi.org/10.1007/s00170-010-2718-z

中文概要

题　目： 连续函数式曲线光滑法

目　的： 用连续函数实现无限接近原始非连续曲线的光滑。

创新点： 首次提出用一个连续函数替代原来由任意多非连续区域函数构成的函数。该方法可视为一种新的函数光滑算法。

方　法： 1. 通过引入特殊的区域变量，并用该区域变量替代原函数自变量的方法，将区域函数改造成在该区域无限接近原函数而在区域外取值常数的函数。2. 把所有的区域函数相乘得到一个连续函数的方程。

结　论： 1. 由任意多非连续区域函数构成的函数可以改造成一个连续函数。2. 该连续函数在原非连续边界的光滑程度可以由各个边界上独立的参数按需调整。3. 该方法产生的连续函数没有摆动现象，其形状与原始区域函数无限接近。该方程在数学上是连续的，同时无限接近原始非连续函数，包括原来在边界上函数值的非连续。

关键词： 曲线光滑；区域变量；区域函数；连续函数

Introducing Editorial Board Member:

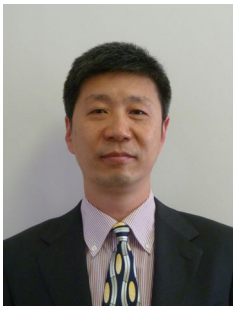

Dr. Yu-fei WU is currently a Professor in Infrastructure Engineering and Metro Chair in the School of Engineering at RMIT University in Australia. He obtained his BSc in 1983 and MSc in 1986 from Zhejiang University, China. He received MEng from National University of Singapore in 1994 and completed his PhD in 2002 at the University of Adelaide, Australia. He has more than ten years of industry working experience in structural engineering as a professional engineer in consulting firms in China, Singapore, and Australia and is a chartered professional engineer of New Zealand and Australia (FIEAust, CPEng, NER, MIPENZ). He worked in Shanghai Jiao Tong University, China from 1989 to 1992 as a lecturer. Prior to joining RMIT University, he was an Associate Professor in the Department of Architecture and Civil Engineering at City University of Hong Kong, China (2004–2015). His research interests lie in the broad field of structural engineering, including concrete structures, structural design, composite structures, fibre-reinforced polymer (FRP) structures, and structural rehabilitation. Prof. WU has received numerous research awards, including the 2018 Moisseiff Award from ASCE. He is the sole or the 1st named inventor of numerous new structural technologies, including six US patents.